# Hierarchical Porous Core−Shell Carbon Nanoparticles

Chang Song,[†,‡] Jianping Du,[†,‡] Jianghong Zhao,[†] Shouai Feng,[†,‡] Guixiang Du,[†,‡] and Zhenping Zhu*,[†]

*State Key Laboratory of Coal Conversion, Institute of Coal Chemistry, Chinese Academy of Sciences, Taiyuan 030001 and Graduate University of Chinese Academy of Sciences, Beijing 100039, China*

*Received October 21, 2008. Revised Manuscript Received February 23, 2009*

The excellent physical and chemical properties of porous carbon materials allow them to be widely used in many fields. Their performance in a specific application is usually determined by structural features such as pore diameter, channel length, and architecture. In recent years, great efforts have been made to develop suitable carbon-based materials with short pores and/or hierarchical porous architectures, for use in transport or diffusion of guest objects by reducing pathways and resistance. In the present paper, we report on a novel carbon nanostructure constructed with a mesoporous core and a microporous shell. The mesopore walls are constructed of only a few graphene layers and can be controllably removed by a wetting oxidation reaction, which leaves behind hollow nanoparticles. These short-pore structures could facilitate the diffusion of molecules; they also show a very high and stable catalytic performance during the dehydrogenation of cyclohexane that is far superior to currently available long-pore materials, such as active carbon and carbon nanotubes.

## Introduction

Porous carbon materials have a number of appealing physical properties, such as low density, high corrosion resistance, tailorable surface properties, and excellent thermal and mechanical stability, that make them useful in many applications, including their use in transport of guest molecules.[1−4] In general, the pore diameter, channel length, and architecture of porous materials usually determine their performance in many applications.[5−9] For example, because many heterocatalytic reactions are kinetically controlled by the diffusion or desorption of products in the pores of the catalysts, catalyst materials with short pores are often required to increase the rate of diffusion of molecules in order to promote the total process.[10] In particular, for multistep chain reactions with intermediates as target products, shortening the pore length of catalysts would be beneficial for instant desorption or diffusion of intermediates, which would effectively avoid overly deep reactions and thus improve reaction selectivity. In the field of electrochemical capacitors, ion transport inside the deep pores of conventional materials is usually limited, which severely reduces charge and discharge rates.[11] Therefore, the development of suitable carbon materials with short pores is now being emphasized to facilitate ion transport by reducing resistance and diffusion pathways.

In general, porous particles with nanoscale sizes represent one candidate in the short-pore material category. In the area of drug delivery, nanosized drug carriers are required to facilitate intracellular drug transport and uptake.[12,13] However, hierarchical porous architectures have many other applications.[6] For example, Cheng et al. reported that carbon materials with three-dimensional aperiodic porous textures exhibit high energy and power density that can be used for electrochemical capacitive energy storage.[14] Zhu et al. recently reported that the application of silica nanoparticles with hollow cores and porous shells can effectively tune and improve drug release and storage capacity.[15] Carbon nanomaterials with similar core−shell structures predictably exhibit unique functions in drug delivery because of their excellent biocompatibility and the tunable properties of porous carbon.[16−21]

The construction of porous structures of carbon particles with sizes in the nanoscale (<100 nm) is usually difficult. Recently, however, the research groups of Hyeon,[22] Lu,[23] and Ikeda,[24,25] were able to successfully synthesize hollow carbon nanoparticles with porous walls through the use of organic polymerization reactions and subsequent carbonization. The construction of the hollow cores was carried out

* Corresponding author. E-mail: zpzhu@sxicc.ac.cn.
† Institute of Coal Chemistry, Chinese Academy of Sciences.
‡ Graduate University of Chinese Academy of Sciences.

(1) Ryoo, R.; Joo, S. H.; Kruk, M.; Jaroniec, M. *Adv. Mater.* **2001**, *13*, 677.
(2) Lee, J.; Kim, J.; Hyeon, T. *Adv. Mater.* **2006**, *18*, 2073.
(3) Wan, Y.; Shi, Y.; Zhao, D. *Chem. Mater.* **2008**, *20*, 932.
(4) Bradley, R. H.; Sutherland, I.; Sheng, E. *J. Colloid Interface Sci.* **1996**, *179*, 561.
(5) Férey, G. *Chem. Soc. Rev.* **2008**, *37*, 191.
(6) Davis, M. E. *Nature (London)* **2002**, *417*, 813.
(7) LaVan, D. A.; McGuire, T.; Langer, R. *Nat. Biotechnol.* **2003**, *21*, 1184.
(8) Rodriguez-reinoso, F. *Carbon* **1998**, *36*, 159.
(9) Vix-Guterl, C.; Frackowiak, E.; Jurewicz, K.; Friebe, M.; Parmentier, J.; Beguin, F. *Carbon* **2005**, *43*, 1293.
(10) Zhang, H.; Sun, J.; Ma, D.; Bao, X.; Klein-Hoffmann, A.; Weinberg, G.; Su, D.; Schloegl, R. *J. Am. Chem. Soc.* **2004**, *126*, 7440.
(11) Li, H. Q.; Luo, J. Y.; Zhou, X. F.; Yu, C. Z.; Xia, Y. Y. *J. Electrochem. Soc.* **2007**, *154*, A731.
(12) Allen, T. M.; Cullis, P. R. *Science* **2004**, *303*, 1818.
(13) Har-el, Y.; Kato, Y. *Curr. Nanosci.* **2007**, *3*, 329.
(14) Wang, D.-W.; Li, F.; Liu, M.; Lu, G. Q.; Cheng, H.-M. *Angew. Chem., Int. Ed.* **2008**, *47*, 373.
(15) Zhu, Y.; Shi, J.; Shen, W.; Dong, X.; Feng, J.; Ruan, M.; Li, Y. *Angew. Chem., Int. Ed.* **2005**, *44*, 5083.

10.1021/cm802852e CCC: $40.75 
Published on Web 03/19/2009

using solid templates such as nanosized silica, titania, or metal salts.[1,2,26] Stein et al. employed dual templates, composed of a block copolymer surfactant and colloidal crystals, to synthesize mesoporous carbon nanoparticles (MSP-3) with different shapes.[27]

In the present paper, we report on core−shell carbon nanoparticles (denoted as CSCNPs) that comprise mesoporous cores and microporous shells. The mesopore walls in the cores are primarily constructed of single or double graphene layers, and can be readily removed, which results in hollow nanoparticles. This carbon nanostructure represents a novel carbon material that has short hierarchical pores. It displays an excellent performance in the platinum-catalytic dehydrogenation of cyclohexane to benzene that is superior to that of carbon materials with long channels, such as active carbon (denoted as AC) and multiwall carbon nanotubes (denoted as MWCNTs) with long channels.

## Experimental Section

The CSCNPs were synthesized by the detonation of a mixture consisting of picric acid, phenol, and cobalt acetate (when used), with desired ratios. The detonation experiments, which were performed in a sealed stainless steel pressure vessel (14 $cm^3$), were initiated by a quick heating (20 °C $min^{-1}$) of the vessel to 310 °C. After the detonation of picric acid, a high-temperature environment (typically 1000 °C) was created inside the vessel, which provided required basic conditions for the decompositions of phenol and cobalt acetate and the construction of the CSCNPs. The entire reaction process was carried out for 10 min, after which the vessel was cooled naturally in air to room temperature. The gaseous products were then emptied and the solid products were collected for further analysis.

For the emptying of the cores of the CSCNPs, 0.4 g of CSCNPs was added to 100 mL of 1.5 M $HNO_3$ and refluxed for 12 h. After the refluxing, the suspension was filtered, washed with deionized water and ethanol, and dried at 100 °C overnight.

The Pt/CSCNP, Pt/AC, and Pt/MWCNT catalysts were prepared by pore volume impregnation of 200 mg of either CSCNP, AC, or MWCNT with an aqueous solution of $PtCl_4$ of the desired solution concentration and volume, followed by vacuum drying at 60 °C overnight. All of the resulting catalysts contained 1 wt % Pt. The pore volumes of the three materials were measured with pure water, and the actually employed volumes of the $PtCl_4$ solution were slightly less than the measured pore volume, to allow the $PtCl_4$ solution to permeate into the pores (or tube channels) as completely as possible. Before the catalysis reactions, the catalysts, loaded in a glass tubular reactor, were reduced in situ by hydrogen at 400 °C for 3 h. After this reduction, the reactor was cooled to and maintained at 310 °C, and cyclohexane was fed into the reactor by a piston pump at a rate of 0.03 mL $min^{-1}$. Cyclohexane concentrations before and during the reaction were analyzed by online gas chromatography, using a thermal conductivity detector and a dioctyl sebacate column.

TEM analyses were performed using a JEM-2010 electron microscope, operated at 200 kV. Surface area and pore analyses, employing $N_2$ as the adsorbate, were carried out at 77.4 K using an ASAP2020 M automated gas-sorption system, which allows a high-resolution adsorption isotherm taken down to $P/P_0 = 1 \times 10^{-8}$. Prior to the measurements, the samples were degassed at 300 °C for 8 h. Powder X-ray diffraction patterns were obtained on a D8 Advance Bruker diffractometer, with Cu Kα radiation.

## Results and Discussion

The CSCNPs were synthesized by detonation-assisted chemical vapor deposition, which we have previously employed to synthesize metal-encapsulated carbon nanoparticles,[28] carbon nanobulbs,[29] and carbon nanotubes.[30−32] In this process, the detonation of the explosive (picric acid) creates the required high-temperature environment in which the premixed carbon/catalyst precursors decompose and then reconstruct as carbon nanostructures. The morphologies of the carbon nanostructures are highly dependent on the type and nature of the carbon/catalyst precursors. Hydrocarbons such as cyclohexane, benzene, and paraffin have been found to be suitable for MWCNT synthesis. In the present synthesis of the CSCNPs, hydroxyl compounds such as phenol, resorcinol, and hexanol were used as carbon precursors. The presence of −OH groups hinders the construction of MWCNTs, and these groups also act as oxidative reagents for pore creation, as occurs during normal carbon activation.[33] Cobalt acetate is used as a catalyst precursor for the catalytic formation of the CSCNP shells. The typical product that is obtained from a mixture of picric acid (2.5 g), cobalt acetate (0.17 g), and phenol (0.53 g) is a black powder with an extremely low apparent density (0.021 $gcm^{-3}$). As observed by transmission electron microscopy (TEM), the product is composed of carbon nanoparticles with a narrow size distribution of 20−60 nm (Figure 1a). Magnified images (Figure 1b) show that the nanoparticles exhibit core−shell structures. Mesopores can be clearly observed within the cores. High-resolution images (Figure 2) reveal that the mesopores have sizes of 2−4 nm and have very thin walls that are composed of only a few graphene layers. The presence of mesopores is also supported by the nitrogen adsorption−desorption isotherm of the product (Figure 3a), which shows the type IV curve with a H3 hysteresis loop,

(16) Yan, A.; Lau, B. W.; Weissman, B. S.; KüLaots, I.; Yang, N. Y. C.; Kane, A. B.; Hurt, R. H. *Adv. Mater.* **2006**, *18*, 2373.
(17) Bianco, A.; Kostarelos, K.; Prato, M. *Curr. Opin. Chem. Biol.* **2005**, *9*, 674.
(18) Smart, S. K.; Cassady, A. I.; Lu, G. Q.; Martin, D. J. *Carbon* **2006**, *44*, 1034.
(19) Fiorito, S.; Serafino, A.; Andreola, F.; Togna, A.; Togna, G. *J. Nanosci. Nanotechnol.* **2006**, *6*, 591.
(20) Parihar, S.; Sharon, M.; Sharon, M. *Synth. React. Inorg. Met.-Org., Nano-Met. Chem.* **2006**, *36*, 107.
(21) Shiba, K. *J. Drug Targeting* **2006**, *14*, 512.
(22) Lee, J.; Kim, J.; Kim, J.; Jia, H.; Kim, M. I.; Kwak, J. H.; Jin, S.; Dohnalkova, A.; Park, H. G.; Chang, H. N.; Wang, P.; Grate, J. W.; Hyeon, T. *Small* **2005**, *1*, 744.
(23) Zheng, T.; Zhan, J.; Pang, J.; Tan, G. S.; He, J.; McPherson, G. L.; Lu, Y.; John, V. T. *Adv. Mater.* **2006**, *18*, 2735.
(24) Ikeda, S.; Ishino, S.; Harada, T.; Okamoto, N.; Sakata, T.; Mori, H.; Kuwabata, S.; Torimoto, T.; Matsumura, M. *Angew. Chem., Int. Ed.* **2006**, *45*, 7063.
(25) Ng, Y. H.; Ikeda, S.; Harada, T.; Higashida, S.; Sakata, T.; Mori, H.; Matsumura, M. *Adv. Mater.* **2007**, *19*, 597.
(26) Lu, A.-H.; Schüth, F. *Adv. Mater.* **2006**, *18*, 1793.
(27) Wang, Z.; Li, F.; Stein, A. *Nano Lett.* **2007**, *7*, 3223.
(28) Lu, Y.; Zhu, Z.; Liu, Z. *Carbon* **2005**, *43*, 369.
(29) Zhu, Z.; Su, D.; Lu, Y.; Schloegl, R.; Weinberg, G.; Liu, Z. *Adv. Mater.* **2004**, *16*, 443.
(30) Lu, Y.; Zhu, Z.; Wu, W.; Liu, Z. *Chem. Commun.* **2002**, *2002*, 2740.
(31) Zhu, Z.; Lu, Y.; Qiao, D.; Bai, S.; Hu, T.; Li, L.; Zheng, J. *J. Am. Chem. Soc.* **2005**, *127*, 15698.

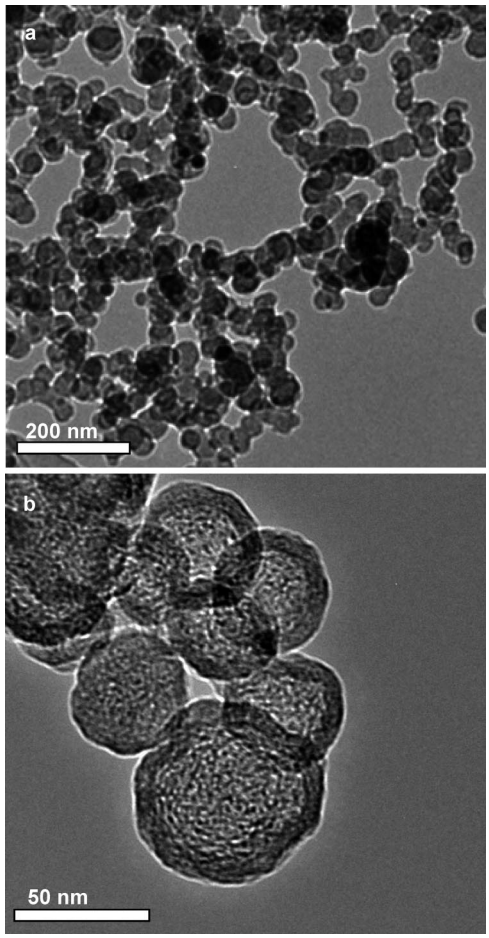


**Figure 1.** (a, b) TEM images of the CSCNPs obtained from a mixture of picric acid (2.5 g), cobalt acetate (0.17 g), and phenol (0.53 g).

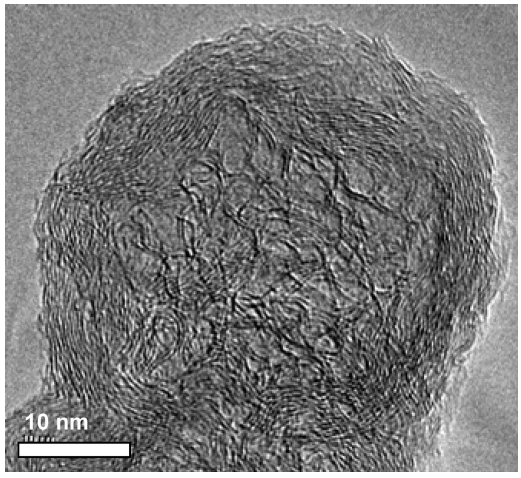


**Figure 2.** A typical high-resolution TEM image of the CSCNPs.

suggesting the occurrence of mesopore-characteristic capillary condensation of nitrogen. The product exhibits a high Brunauer−Emmett−Teller (BET) surface area (668 $m^2\ g^{-1}$) and a very large pore volume (0.93 $cm^3 g^{-1}$). The nitrogen accessibility of the mesopores in the cores indicates that the shells also possess a porous structure, which provides the

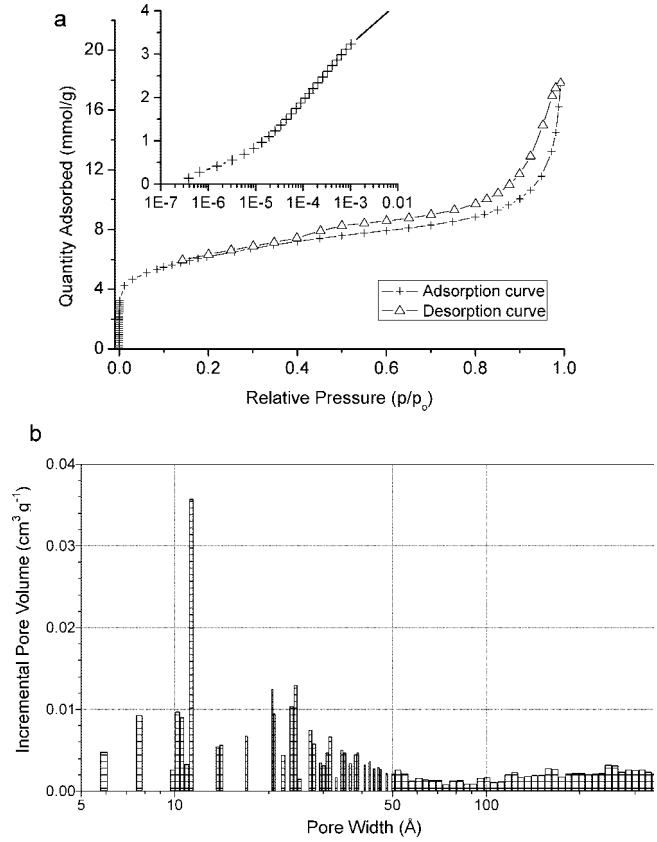


**Figure 3.** (a) High-resolution nitrogen adsorption−desorption isotherm of the CSCNPs. Inset is magnified adsorption curve at low $P/P_0$. (b) Pore size distribution histogram determined by DFT method.

required windows for the entrance of nitrogen molecules into the cores. The invisible feature of the shell pores by TEM and the presence of plentiful structural defects on the graphitic shells (Figure 2) suggest that the pores on the shells are micropores. The nitrogen adsorption curve of the CSCNPs (a magnified curve from $1 \times 10^{-7}$ to $1 \times 10^{-2}$ of $P/P_0$ is presented in the inset of Figure 3a) shows a strong adsorption at low $P/P_0$, indicating that micropores are evident in the CSCNPs. The calculated t-plot micropore area is 223 $m^2\ g^{-1}$. The pore size distribution calculated by the density function theory (DFT) method is presented in Figure 3b. Clearly, the CSCNPs contain both mesopores and micropores. The sizes of micropores peaked at about 1.1 nm, whereas the sizes of mesopores were predominantly in the range of 2−5 nm, in close agreement with the TEM observations.

The nanoparticles obtained without cobalt catalysts show no obvious shells, as observed by TEM (Figure 4). Under TEM, the mesoporous structures are still evident, with a size distribution similar to the sample obtained by cobalt catalysts. This indicates the importance of metal catalysts in the formation of the shells of the CSCNPs. Considering that the energy for the present formation of the CSCNPs is provided by the detonation of picric acid and is determined by the loading density of picric acid, we have tried to tailor the shell thickness by adjusting detonation recipes. Typically, when the amount of picric acid is reduced from 2.5 to 1.5 g (with the amounts of carbon and cobalt precursors remaining

(32) Du, G.; Feng, S.; Zhao, J.; Song, C.; Bai, S.; Zhu, Z. *J. Am. Chem. Soc.* **2006**, *128*, 15405.
(33) Luh, T. Y.; Leung Mk, M. K.; Wong, K. T. *Chem. Rev.* **2000**, *100*, 3187.

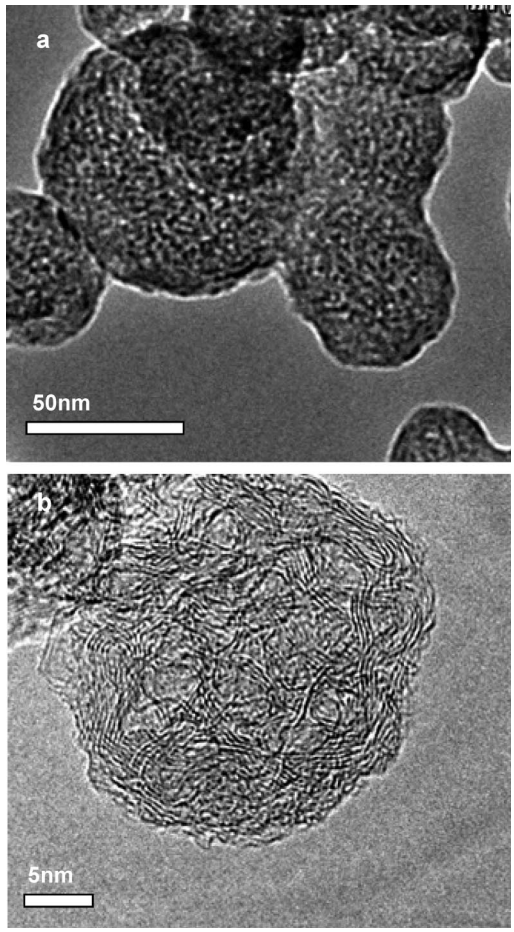


**Figure 4.** Nanoparticles obtained from a mixture of the picric acid (2.5 g) and phenol (0.53 g), without catalysts.

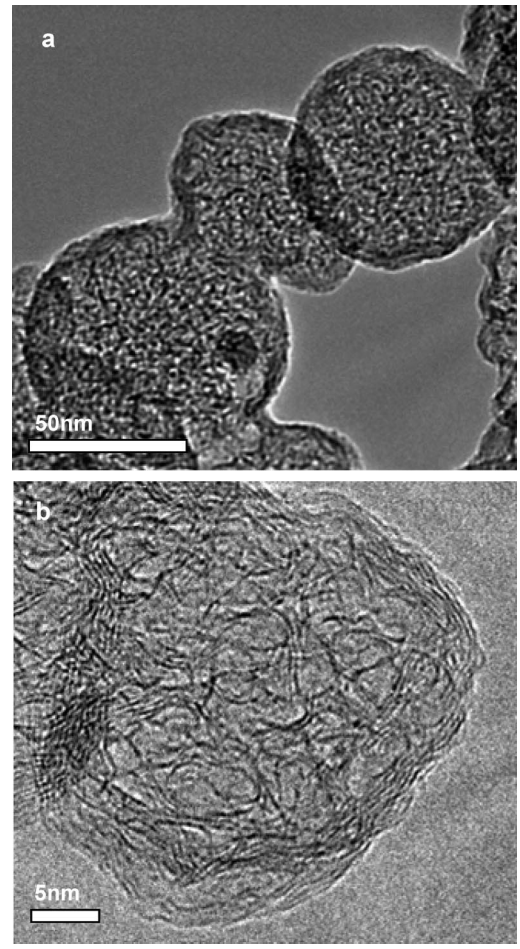


**Figure 5.** CSCNPs obtained from a mixture of picric acid (1.5 g), cobalt acetate (0.17 g), and phenol (0.53 g).

unchanged), the resulting nanoparticles exhibit significantly thinner shells, on which more structural defects are generated (Figure 5). The sizes of the mesopores in the cores and the thickness of pore walls show no visible changes.

As described above for the CSCNPs obtained, the shells are constructed by multilayer graphitic structure containing micropores, whereas the mesopore walls in the cores are constructed by only a few graphene layers. These are also highly different in size and structural extensiveness, which theoretically results in a significant difference in structure curving tension. In addition, the graphitic shells are actually formed by the catalyzed transformation and crystallization from the mesopore structures. Thus, they have fewer structural defects than do the mesopore walls.

These structural differences between the shells and the mesopore walls predictably induce a difference in their chemical reactivity, which guided us to reform the CSCNPs into hollow carbon nanoparticles by controllably eliminating the mesopore walls with an oxidative acid. The micropores on the shells provide the required windows for the access of the acid molecules into the cores. Following this strategy, hollow carbon nanoparticles can be successfully obtained by treating the CSCNPs with concentrated nitric acid, as shown in Figure 6a. The mesopore walls are completely removed, whereas the shells still remain, although somewhat structurally degraded, leaving behind entirely hollow cores (Figure 6). The inner diameter of the hollowed nanoparticles is generally in the range of 25−40 nm and the outer diameter is in the range of 35−45 nm (Figure 7). The nitrogen adsorption−desorption isotherm of the hollowed nanoparticles (Figure 8a) was similar to a type IV curve with an obvious mesopore-characteristic H3 hysteresis loop, in agreement with the TEM observation of the hollowed cores. The BET specific surface area of the hollowed nanoparticles was reduced from 668 to 255 $m^2\ g^{-1}$, and thus was likely linked with the loss of the surfaces originally contributed by the thin-graphene-layer mesopore walls in the CSCNPs. The clear adsorption in the range of low $P/P_0$ (the inset of Figure 8a shows a magnified adsorption curve from $1 \times 10^{-7}$ to $1 \times 10^{-2}$ of $P/P_0$) suggests that the hollowed carbon nanoparticles still contain micropores, most likely on the shells. Figure 8b presents the DFT-calculated pore size distribution of the hollowed particles. Clearly, the mesopores of 2−5 nm that are presented in the original CSCNPs disappear, consistent with the TEM observations and the acid erosion of the mesopores in the cores. Compared to the original CSCNPs, the hollowed particles seemed to exhibit larger micropore sizes, possibly associated with a pore widening during the acid treatment. These results further confirm that the shells of the original and hollowed CSCNPs have a porous structure, through which the liquid acid can readily enter into the CSCNP cores for the erosion of the mesopore walls.

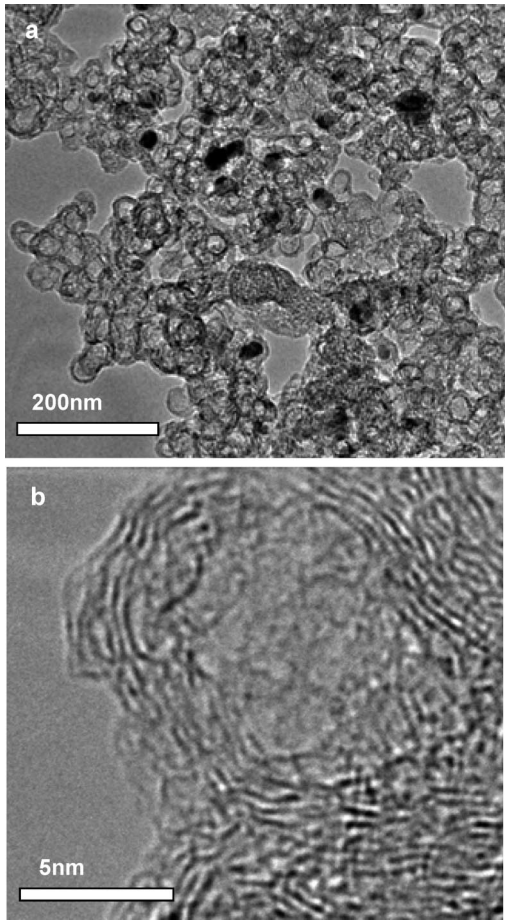


**Figure 6.** TEM images of the hollow particles obtained by a $HNO_3$ treatment of CSCNPs.

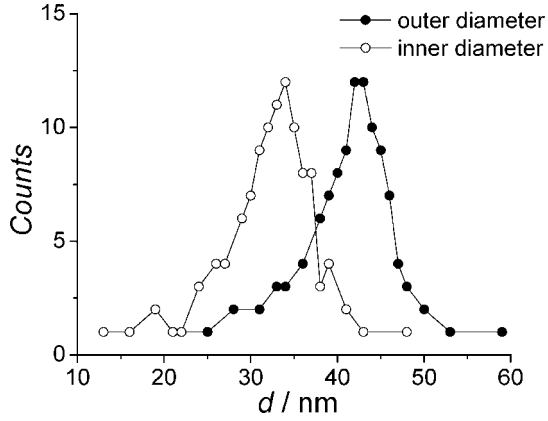


**Figure 7.** Inner/outer diameter distributions of the hollow particles obtained by a $HNO_3$ treatment of CSCNPs.

The short-pore feature of the CSCNPs may endow them with unique properties and possibly with potential advantages in applications such as catalysis, drug delivery, electrochemical capacitors, chemical separations, and sensors. As a demonstration, we have explored the catalytic dehydrogenation of cyclohexane to benzene, using a CSCNP-supported platinum catalyst. This reaction, as a key step in the benzene−cyclohexane−benzene reaction cycle, is a promising process for chemical hydrogen storage.[34−36] In the reaction cycle, the benzene−cyclohexane hydrogenation reaction moiety is the easiest to be performed and has been industrialized. In contrast, some problems in the cyclohexane−benzene dehydrogenation reaction moiety remain, such as the high-temperature requirement and catalyst deactivation.[37−41] The deactivation is mainly derived from the formation of cokes over the catalyst surfaces, which heavily contaminate the catalyst active sites. This coke formation is generally induced by strong adsorption and long retention time of the product benzene over catalyst surfaces,[42−46] which become poor carbon-supported catalysts because of the strong $\pi-\pi$ interaction between carbon materials and benzene.[47] Intrinsically, decreasing the adsorption and residence time

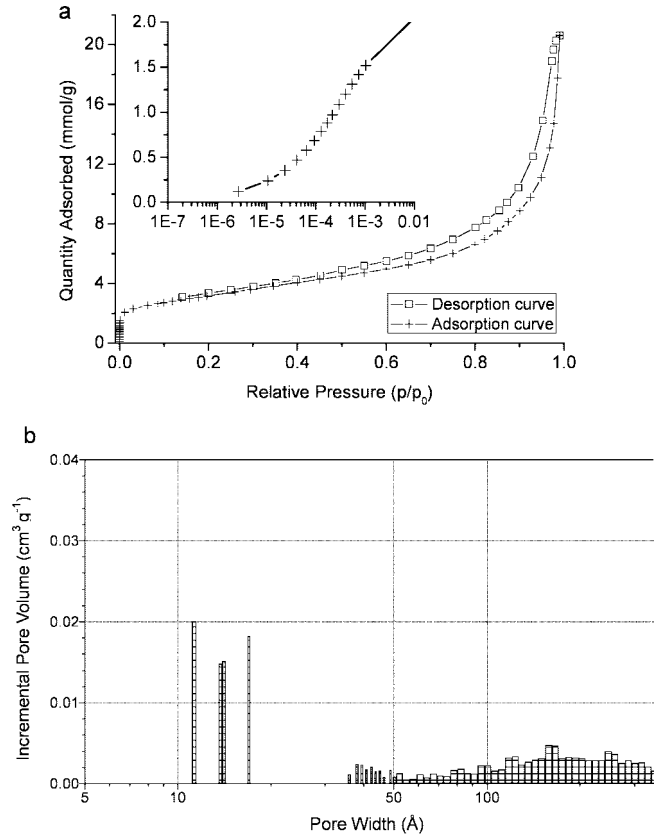


**Figure 8.** (a) High-resolution nitrogen adsorption−desorption isotherm the particles hollowed by a $HNO_3$ treatment. The inset is magnified adsorption curve at low $P/P_0$. (b) Pore size distribution histogram determined by DFT method.

(34) Yamamoto, S.; Hanaoka, T.; Hamakawa, S.; Sato, K.; Mizukami, F. *Catal. Today* **2006**, *118*, 2.
(35) Itoh, N.; Xu, W. C.; Hara, S.; Sakaki, K. *Catal. Today* **2000**, *56*, 307.
(36) Sebastian, D.; Bordeje, E. G.; Calvillo, L.; Lazaro, M. J.; Moliner, R. *Int. J. Hydrogen Energy* **2008**, *33*, 1329.
(37) Maatman, R. W.; Mahaffy, P.; Hoekstra, P.; Addink, C. *J. Catal.* **1971**, *23*, 105.
(38) Surangalikar, H.; Ouyang, X.; Besser, R. S. *Chem. Eng. J.* **2003**, *93*, 217.
(39) Aboul-Gheit, A. K.; Aboul-Fotouh, S. M.; Aboul-Gheit, N. A. K. *Appl. Catal., A* **2005**, *283*, 157.
(40) Vilella, I. M. J.; de Miguel, S. R.; Scelza, O. A. *J. Mol. Catal. A-Chem.* **2008**, *284*, 161.
(41) Lytken, O.; Lew, W.; Campbell, C. T. *Chem. Soc. Rev.* **2008**, *37*, 2172.
(42) Zharkov, B. B.; Medzhinskii, V. L.; Butochnikova, L. F.; Oranskaya, O. M.; Maryshev, V. B. *Chem. Technol. Fuels Oils* **1988**, *24*, 157.
(43) Marécot, P.; Akhachane, A.; Barbier, J. *Catal. Lett.* **1996**, *36*, 37.
(44) Ali, L. I.; Ali, A.-G. A.; Aboul-Fotouh, S. M.; Aboul-Gheit, A. K. *Appl. Catal., A* **1999**, *177*, 99.
(45) Albers, P.; Pietsch, J.; Parker, S. F. *J. Mol. Catal., A* **2001**, *173*, 275.
(46) Carrott, P. J. M.; Ribeiro Carrott, M. M. L.; Cansado, I. P. P.; Nabais, J. M. V. *Carbon* **2000**, *38*, 465.
(47) Sinnokrot, M. O.; Valeev, E. F.; Sherrill, C. D. *J. Am. Chem. Soc.* **2002**, *124*, 10887.

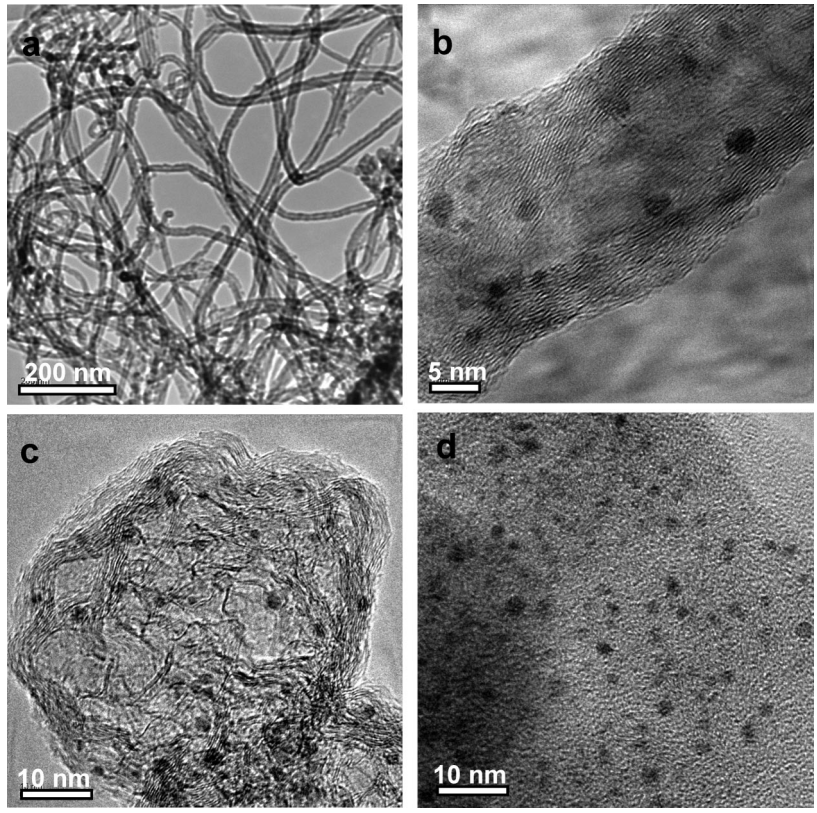


**Figure 9.** (a) TEM images of carbon nanotubes with long channels. (b, c, d) TEM images of Pt/MWCNT, Pt/CSCNP, and Pt/AC catalysts, showing that the platinum nanoparticles are well-dispersed in both cases and exhibit similar sizes.

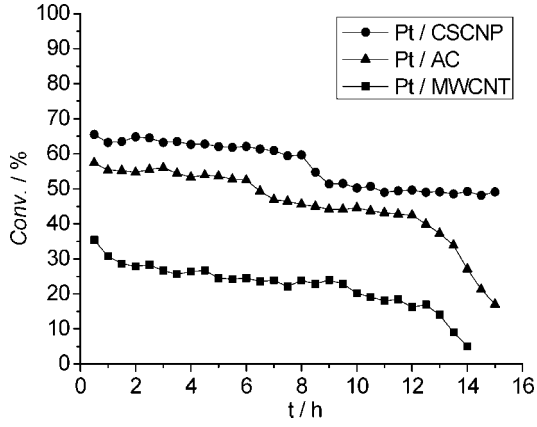


**Figure 10.** Cyclohexane conversions over Pt/CSCNP, Pt/AC, and Pt/MWCNT catalysts as a function of reaction duration.

of benzene would be beneficial to the improvement of catalyst stability. One may imagine that, for short-pore materials with a short diffusion pathway, molecules can more easily "escape" from these surfaces by significantly shortening the stay time. Following this idea, we have demonstrated the catalytic cyclohexane-benzene dehydrogenation reaction over Pt/CSCNP catalyst, and compared its catalytic performance with those of the Pt catalysts supported on AC and MWCNTs, which typically exhibit long pores or channels (Figure 9a for MWCNTs).

Figure 10 shows that the catalytic activity of the Pt/CSCNP catalyst is significantly higher than that of either the Pt/AC or the Pt/MWCNT catalysts, with the initial cyclohexane-benzene conversions being 65.5%, 57.4%, and 35.4%, respectively. Notably, the Pt/AC and Pt/MWCNT catalysts quickly became deactivated as the reaction duration progressed, with continuous and obvious drops in cyclohexane−benzene conversion. The drops become more rapid after 12 h of reaction time, with a drop in cyclohexane−benzene conversion from 57.4 to 17.0% (within 15 h) observed for the Pt/AC catalyst, and from 35.4 to 4.6% (within 14 h) for the Pt/MWCNT catalyst. Interestingly, although the Pt/CSCNP catalyst also initially exhibits somewhat of a deactivation, it finally stabilizes during further reactions and then maintains a relatively high cyclohexane−benzene conversion, at about 49%.

As shown by TEM observations (Figure 9b−d), the size of platinum catalyst particles is in the range of 1−3 nm, independent of the support material. In addition, XRD analyses indicate that for all three catalysts, the crystal structures of the platinum catalyst particles are similar, with a face-centered cubic structure (Figure 11). The obvious difference among the three catalysts is their pore structures. The CSCNPs exhibit a short-pore feature (below 40 nm, estimated from the size of the CSCNPs), whereas the AC is a bulk-sized porous material, showing deep pores, and the MWCNTs have micrometer-scale long channels (Figure 9a). It is therefore possible that the unique short pore structure of the CSCNPs plays an important role in the improvement of the catalytic activity and stability, through facilitating the diffusion and escape of product benzene molecules from the catalyst surfaces, thus shortening their stay time and reducing coke formation. Indeed, regarding the improvement of Pt/CSCNP activity, the contributions of other factors are difficult to exclude because activity is often highly sensitive

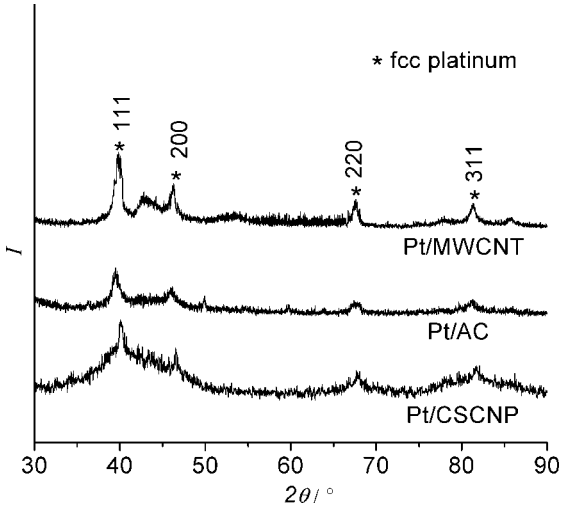


**Figure 11.** X-ray diffraction patterns of the Pt/MWCNT, Pt/AC, and Pt/CSCNP catalysts, showing that the platinum nanoparticles exhibit the same crystal structure in all cases.

to the sizes and microstructures of both the catalyst particles and the support materials.

In general, an identification of the relationship between pore length and catalyst stability is less affected by other factors. Strictly speaking, selectively filling Pt nanoparticles into the pores (or tube channels) rather than onto the outer surfaces would be better for an exact identification of the relationship between the short pore structure and the improved catalytic performance of the CSCNPs. For this purpose, during the impregnation preparations of the catalysts, we employed a $PtCl_4$ solution slightly less than the pore volume to allow it to permeate into the pores (or tube channels) as completely as possible. From the TEM observations (Figure 9b−d), the outer surfaces of the Pt-loaded CSCNPs, MWCNTs, and ACs were relatively clean, suggesting that Pt nanoparticles appear to mainly stay in the pores, and only a minority locate on the outer surfaces. Therefore, catalyst stability is chiefly determined by the event of pore-filling with active Pt particles for all three catalysts, and the difference in their pore length is likely to be responsible for significant changes in stability. More detailed studies are currently under way in our laboratory to confirm this.

## Conclusion

In summary, novel carbon nanoparticles, constructed by mesoporous core and microporous shells, have been synthesized by a one-step process that is based on detonation-assisted chemical vapor deposition. The mesopore walls consist of a few graphene layers and can be controllably removed by a wetting oxidation treatment, leaving behind hollow nanoparticles. The porous core−shell nanostructures provide ideal short pores (superior to the active carbon and carbon nanotubes with long channels), where the catalytic reactions that are controlled by the desorption or diffusion of product molecules can proceed more stably. Additionally, the unique carbon nanostructures may have a number of applications, for example, in drug delivery, chemical separations, electrochemical capacitor, and sensor to tailor or improve material functions.

**Acknowledgment.** This work was financially supported by Natural Science Foundation of China (20673135, 50702065) and Chinese Academy of Sciences following the "Bairen" program. The authors also gratefully thank Prof. Weibin Fan for his discussion on the nitrogen adsorption−desorption analyses.

CM802852E